ACS OMEGA

http://pubs.acs.org/journal/acsodf

Article

# Morphology Control via RAFT Emulsion Polymerization-Induced Self-Assembly: Systematic Investigation of Core-Forming Blocks

Atsushi Takashima, Yasushi Maeda, and Shinji Sugihara*

Cite This: *ACS Omega* 2022, 7, 26894−26904

Read Online

ACCESS | Metrics & More | Article Recommendations | Supporting Information

**ABSTRACT:** Polymerization-induced self-assembly (PISA) is a useful formulation for readily obtaining nanoparticles from block copolymers in situ. Reversible addition−fragmentation chain-transfer (RAFT) emulsion polymerization is utilized as one of the PISA formulations. Various factors have so far been investigated for obtaining nonspherical particles via RAFT emulsion polymerization, such as the steric structure of the shell, the glass-transition temperature ($T_g$) of the core-forming block, and the water solubility of the core-forming monomer. This study focuses on core-forming blocks without changing the structure of the shell-forming block. In particular, we elucidate the balance between $T_g$ for the core-forming block and the water solubility of the core monomer. A series of alkyl methacrylates, such as methyl methacrylate (MMA), ethyl methacrylate (EMA), and *n*-propyl methacrylate (PrMA), are emulsion-polymerized in the presence of a poly[poly(ethylene glycol) methyl ether methacrylate] (PPEGMA) macromolecular chain-transfer agent via the RAFT process. The resulting in situ morphology changes to form shapes such as spheres, worms (toroids), and vesicles are systematically investigated. The properties of the core that determine whether a morphological change occurs from spheres are (i) the solubility of the core-forming monomer in water, (ii) the relationship between $T_g$ for the core-forming block and the polymerization temperature, and (iii) the hydrophobic core volume, which changes the packing parameter. These factors allow prediction of the block copolymer morphology produced during RAFT emulsion polymerization of other methacrylates such as *n*-butyl methacrylate (BuMA), tetrahydrofurfuryl methacrylate (THFMA) with physical properties of the homopolymer (poly(tetrahydrofurfuryl methacrylate) (PTHFMA)) between those for poly(MMA) (PMMA) and PBuMA, and 1-adamantyl methacrylate (ADMA) with low monomer solubility in water and high $T_g$ of the homopolymer (PADMA).

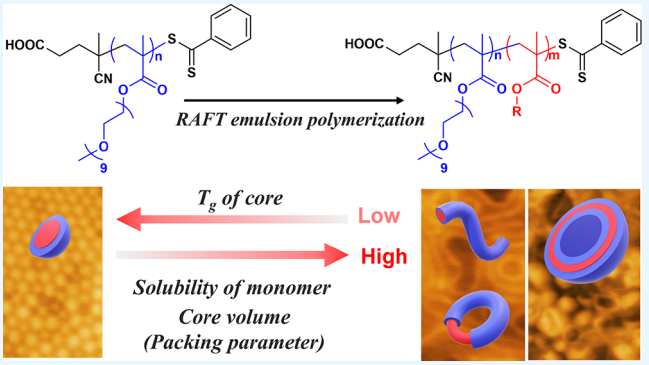


## INTRODUCTION

Polymerization-induced self-assembly (PISA) refers to the formation of nanoparticles such as spheres, worms, and vesicles through the synthesis of amphiphilic block copolymers and in situ self-assembly.[1−9] Compared to the conventional self-assemblies of block copolymers in selective solvents,[10] various nanoparticles can be obtained in a straightforward one-pot approach while facilitating high yield and scalability, which is industrially advantageous. In principle, since nanoparticles are obtained simultaneously with polymerization and can be used as they are, a metal-free system such as reversible addition−fragmentation chain-transfer (RAFT) polymerization[11,12] that does not require purification has mostly been employed (Scheme 1).

In block copolymerization using RAFT polymerization, a macromolecular chain-transfer agent (macro-CTA) is synthesized at the first stage. The resulting polymer corresponds to the shell and stabilizer of the nanoparticles. Subsequently, polymerizing a second-stage monomer using the resultant macro-CTA allows for the synthesis of block copolymers. In PISA, nano-organization is performed using the second-stage monomer as the core-forming block. Thus, there are many examples of PISA via RAFT dispersion polymerization or RAFT emulsion polymerization without metallic catalysts. The former is reflected in the morphology given by the diblock copolymer composition, i.e., relative block volume fractions, because polymerization starts in a homogeneous system. The morphological change is generally controlled by the relative volume ratio of blocks, i.e., the packing parameter.[13,14] This roughly corresponds to the blockchain length ratio. Furthermore, the morphology depends on polymerization conditions such as the concentration of solids and additives. Many reports have been published on the synthesis of nanoparticles with various morphologies.[15−26] However, a special monomer is required

Received: June 2, 2022
Accepted: July 14, 2022
Published: July 25, 2022

**Scheme 1. RAFT Aqueous Emulsion Polymerization of MMA, EMA, PrMA, BuMA, THFMA, and ADMA Using the PPEGMA Macro-CTA at 70 °C**[a]

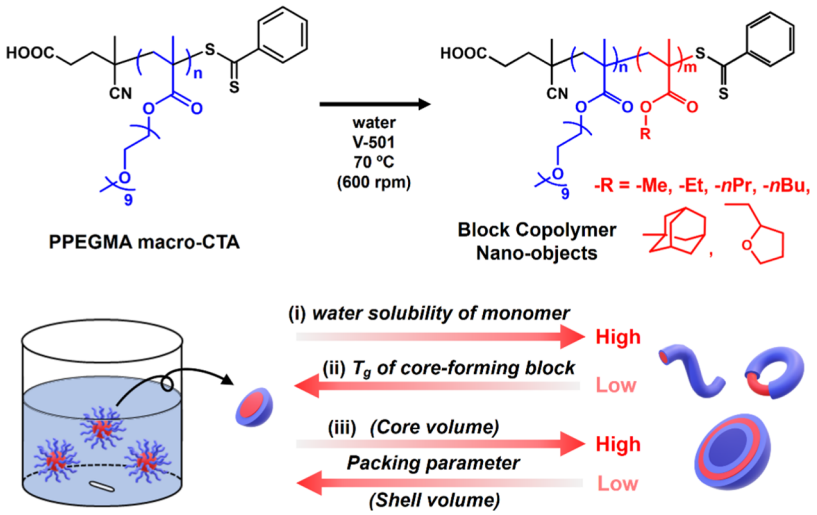


[a]The properties of the core that determine whether a morphological change occurs from spheres to worms, toroids, or vesicles: (i) the solubility of the core-forming monomer in water, (ii) the relationship between $T_g$ for the core-forming block and the polymerization temperature, and (iii) the hydrophobic core volume, which changes the packing parameter.

in an aqueous dispersion system because the monomer must be soluble in water, while the polymer product must be insoluble in water.

Emulsion polymerization is also a useful process because it can be applied to a large number of hydrophobic monomers. However, there are not as many examples describing the synthesis of higher-order structures other than spheres, such as worms and vesicles, as for the case of dispersion polymerization. However, there are some reports of successful synthesis of nanoparticles by emulsion polymerization focusing on the hydrophilic part or the hydrophobic moiety. Charleux et al. first reported RAFT emulsion polymerization of styrene to produce nanoparticles such as spheres, worms, and vesicles using a poly[(ethylene glycol) methyl ether (meth)acrylate-*co*-(meth)-acrylic acid] macro-CTA as an ionic shell.[27−30] These studies showed the effect on the block copolymer morphology in water due to changes in pH and salt concentration. Using a similar macro-CTA, other groups investigated the effect of end-group hydrophobicity[31] and the random incorporation of a hydrophilic component.[31−34] D'Agosto et al. succeeded in synthesizing polystyrene (PSt) nanoparticles with various morphologies by controlling the topology of the macro-CTA of poly(*N*-acryloylmorpholine) with poly[poly(ethylene glycol) acrylate].[35] In addition, molecular dynamics simulations revealed that attractive interactions of poly(ethylene glycol) side chains had a significant effect on morphological changes.[36] Sugihara et al. focused on the relatively high hydrophilic−lipophilic balance (HLB) of these macro-CTAs that succeeded in preparing various nanoparticles. Using a nonionic poly[di(ethylene glycol)vinyl ether] macro-CTA with HLB = 15.4, they synthesized poly(vinyl acetate) nanoparticles via RAFT emulsion polymerization.[37] Thus, a well-designed macro-CTA as a shell has the potential to provide various nanoparticles in RAFT emulsion polymerization.

Armes et al. carried out a series of studies focusing on the core of the hydrophobic moiety. They performed RAFT emulsion polymerization of a 2-hydroxybutyl methacrylate using poly-[(meth)acrylic acid] macro-CTA and revealed that the aqueous solubility of the core-forming monomer is an important factor that affects the resulting morphology.[38,39] Similarly, the effects of the core-forming monomer structure and solubility on the morphology were investigated using α-hydroxymethyl acrylate.[40] Hatton and Armes et al. then used poly(glycerol monomethacrylate) (PGMA) to emulsion-polymerize glycidylryl (GlyMA) [aqueous solubility (soly.) = 26.7 g/L at 60 °C, $T_g$ of homopolymer = 45 °C] which is relatively soluble in water, to selectively obtain worms.[41,42] Tan et al. focused on the solubility and glass-transition temperature ($T_g$) of the core-forming monomers.[43] They conducted RAFT emulsion polymerization using a poly[poly(ethylene glycol) methyl ether methacrylate] (PPEGMA) macro-CTA. The monomers were GlyMA, methyl methacrylate (MMA, soly. = 22.5 g/L at 60 °C, $T_g$ = 125 °C), and benzyl methacrylate (soly. = 0.4 g/L at 70 °C, $T_g$ = 54 °C). They concluded that the aqueous solubility of monomers and the $T_g$ values for the generated polymers are the two key factors that affect the morphological evolution under RAFT-mediated emulsion polymerization conditions. However, there have been no systematic studies on the effects of the $T_g$ of the core-forming block and solubility balance on the morphology in RAFT emulsion polymerization.

Therefore, we first performed RAFT emulsion polymerization of three types of monomers: MMA, ethyl methacrylate (EMA), and propyl methacrylate (PrMA) at 70 °C using PPEGMA macro-CTA. As shown in Table 1, the descending order of $T_g$'s of the homopolymers is poly(MMA) (PMMA), poly(EMA)

**Table 1. Properties of Poly(alkyl methacrylate) for Core-Forming Block**[a]

| core-forming block | PMMA | PEMA | PPrMA | PBuMA |
|---|---|---|---|---|
| alkyl carbon number | 1 | 2 | 3 | 4 |
| $T_g$ (°C) | 125 | 60 | 35 | 20 |
| soly. of monomer (g/L)[b] exp. [calcd[c]] | 15 [25] | 5.4 [11] | −[5.5] | 0.8 [2.6] |

[a]Refs 44−46. [b]Aqueous solubility at 25 °C. [c]Calculated data from Advanced Chemistry Development (ACD/Labs).



https://doi.org/10.1021/acsomega.2c03440
ACS Omega 2022, 7, 26894−26904

(PEMA), and poly(PrMA) (PPrMA), and the solubilities of the monomers in water are MMA, EMA, and PrMA in descending order. In order for a morphology change to occur during emulsion polymerization, it is necessary for the $T_g$ of the core-forming block to be relatively low with respect to the polymerization temperature, and the aggregates must be ergodic (dynamic). Moreover, the solubility of the core-forming monomer in water needs to be relatively high. This is because kinetically trapped spheres derived from the monomer droplets are not formed. In other words, it is important to achieve emulsion polymerization conditions that are closer to those for a dispersion polymerization system. As an alternative scenario, the morphological transition was caused by kinetically trapped sphere−sphere fusion.[6,24] Based on these results, morphology changes were also predicted and investigated using three types of core-forming blocks such as poly(butyl methacrylate) (PBuMA) with a longer alkyl chain, poly(tetrahydrofurfuryl methacrylate) (PTHFMA) with physical properties between those for PEMA and PPrMA, and poly(1-adamantyl methacrylate) (PADMA) with a high $T_g$ for the homopolymer and a low monomer solubility in water.

## EXPERIMENTAL SECTION

**Materials.** 4-Cyano-4-(thiobenzoylthio)pentanoic acid (CADB) was synthesized according to a literature protocol.[47] 4,4′-Azobis (4-cyanopentanoic acid) (V-501, FUJIFILM Wako >98.0%) was used as received. Poly[(ethylene glycol) methyl ether methacrylate] (PEGMA, Sigma-Aldrich; average $M_n$ = 500 g/mol, 9 EO units), MMA (FUJIFILM Wako; >98.0%), EMA (FUJIFILM Wako; >99.0%), PrMA (FUJIFILM Wako; >96.0%), BuMA (TCI; >99.0%), tetrahydrofurfuryl methacrylate (THFMA, TCI; >98.0%), and ethylene glycol dimethacrylate (EGDMA, Sigma-Aldrich; 98%) were purified using the corresponding inhibitor removers prepacked columns (Sigma-Aldrich). 1-Adamantyl methacrylate (ADMA) was kindly donated by Osaka Organic Chemical Industry, Ltd. For solvents, dry 1,4-dioxane (FUJIFILM Wako; >99.5%, water < 10 ppm) and ultrapure water (FUJIFILM Wako) were used as received.

**Synthesis of PPEGMA Macro-CTA.** RAFT solution polymerization of PEGMA was performed in 1,4-dioxane at $[PEGMA]_0/[CADB]_0/[V\text{-}501]_0$ = 20:1:0.125 (molar ratio) and $[PEGMA]_0$ = 25 wt %. PEGMA (10.0 mmol, 5.00 g; target degree of polymerization (DP) of 20), CADB (0.50 mmol, 139.7 mg), V-501 (0.0625 mmol, 17.5 mg), and 1,4-dioxane (14.84 g) were added to a 100 mL Schlenk flask with a magnetic stir bar. The reaction mixture was degassed over three freeze−pump−thaw (FPT) cycles, and then the flask was filled with nitrogen. The solution was stirred in a preheated oil bath at 70 °C for a day. The polymerization mixture was quenched by cooling in an ice water bath and exposure to air. The product was purified by dialysis against deionized water using semipermeable cellulose tubing (SPECTRA/POR, corresponding to a molecular weight cutoff of 3500 Da) and then freeze-dried to obtain pure PPEGMA macro-CTA. The number-average molecular weight ($M_n$) and polydispersity ($M_w/M_n$, $M_w$: weight-average molecular weight) were determined via size exclusion chromatography (SEC). The DP for the macro-CTA was determined by the area of phenyl signals (7.3−8.1 ppm) on RAFT-end group and methyl signal (3.3−3.45 ppm) on PEGMA side chain using $^1$H NMR spectroscopy.

**RAFT Emulsion Polymerization of Core-Forming Monomer.** All RAFT emulsion polymerizations were performed using the following protocol. In the case of the polymerization of EMA for a target DP = 100 of PEMA, $PPEGMA_{19}$ macro-CTA (0.024 mmol, 0.238 g) was mixed with V-501 (0.0035 mmol, 1.0 mg), EMA (2.81 mmol, 0.321 g; target DP of 100), and pure water (2.4 g) at $[macro\text{-}CTA]_0/[EMA]_0/[V\text{-}501]_0$ = 1:100:0.125 (molar ratio) and 20 wt % solid concentration in a Schlenk tube. The solid concentration corresponds to the final copolymer concentration in water, which is defined as [PPEGMA macro-CTA (g) + core-forming monomer (g)]/[total reaction mixture (g)] × 100. Since the solution pH was ca. 3.50, the RAFT-end group is −COOH. The mixture was degassed over three FPT cycles, and then the tube was filled with nitrogen. Polymerization was started at 70 °C, with stirring at 600 rpm using a magnetic stir bar. After the desired time, the polymerization mixture was quenched by cooling to room temperature and exposure to air. The monomer conversion was estimated from the residual EMA monomer in the resultant latex by $^1$H NMR spectroscopy, which was determined by the area of vinyl signals (6.0−6.1 ppm) of EMA monomer and methyl signals (1.1−1.4 ppm) of PEMA using $^1$H NMR spectroscopy.

**General Polymer Characterization.** $^1$H NMR spectra were recorded on JEOL JNM-ECX500II (500 MHz) spectrometer in $d_4$-methanol, a $d_4$-methanol/$CDCl_3$ mixture, or $D_2O$. For example, the resulting dispersion after polymerization was diluted by $D_2O$ to ca. 1 wt % before measurement. Furthermore, for the determination of the DP, the resulting emulsion was partially evaporated and diluted with $d_4$-methanol or $d_4$-methanol/$CDCl_3$ mixture. The molecular weight distribution (MWD) was assessed by SEC in tetrahydrofuran using polystyrene (PSt) gel columns [TSK guard column $H_{XL}$-L + TSKgel $GMH_{HR}$-M × 3; flow rate: 1.0 mL/min] connected to a Waters e2695 with 2489 UV/Vis and 2414 RI detectors. $M_n$ and $M_w/M_n$ were calculated from the SEC curves based on PMMA calibration standards. Dynamic light scattering (DLS) measurements of ca. 0.5 wt % diluted latex were performed using a Malvern Zetasizer Nano-ZSP instrument at 25 °C. The scattered light was detected at an angle of 173°. The mean particle diameter ($D_h$) and polydispersity index (PDI) for the nanoparticles were calculated by cumulant analysis of the experimental correlation function using Zeta Software version 7.04. The results were averaged over 16 consecutive runs. The morphology of the resulting block copolymer in the emulsion was observed by scanning probe microscopy (SPM-9700, Shimadzu) with a silicon probe (Olympus, OMCL-AC160TS-C3), which had a resonance frequency of 300 kHz and a spring constant of 26 N/m. The morphology was observed as a height image by atomic force microscopy (dynamic-mode AFM) at ambient temperature. The sample for AFM height imaging was prepared as follows: muscovite mica (V-4 grade, Alliance biosystems) cut to a 1 × 1 $cm^2$ section was taped on a steel mounting disc 12 mm in diameter, and 20 $\mu$L of the resulting latex solution diluted in water (ca. 0.05 wt %) was dropped on the mica, and then the sample was air-dried for a day.

## RESULTS AND DISCUSSION

**Synthesis of PPEGMA Macro-CTA.** PPEGMA macro-CTA was prepared from RAFT solution polymerization of PEGMA monomer in 1,4-dioxane at 70 °C for 24 h using CADB as a RAFT agent and V-501 as an azo-initiator: $[PEGMA]_0/[CADB]_0/[V\text{-}501]_0$ = 20:1:0.125 (molar ratio). The monomer conversion was calculated from diluted aliquots of the as-quenched reaction mixture using $^1$H NMR spectroscopy in $CDCl_3$ by comparing the integrated monomer vinyl resonances


https://doi.org/10.1021/acsomega.2c03440
ACS Omega 2022, 7, 26894−26904

at 5.5−6.2 ppm to the signal due to methylene groups next to the ester in PEGMA at 4.0−4.4 ppm. The quenched mixture was diluted using water, followed by dialysis against deionized water using semipermeable cellulose tubing for a day, and PPEGMA macro-CTA was isolated by lyophilization. DP (=$n$) of PPEGMA obtained here was 19, i.e., $PPEGMA_{19}$ macro-CTA, which was estimated from the monomer conversion (conv. = 96%). The MWD by SEC and $^1$H NMR result of $PPEGMA_{19}$ macro-CTA are shown in Figures 1 and S1 of the Supporting Information, respectively.

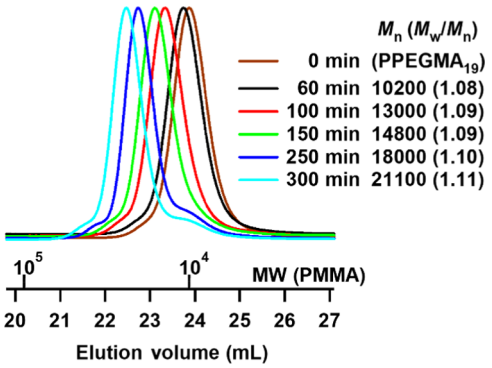


**Figure 1.** SEC traces at each polymerization time for the targeted $PPEGMA_{19}$-$b$-$PEMA_{100}$ nanoparticles via RAFT emulsion polymerization of EMA using $PPEGMA_{19}$ macro-CTA: $[EMA]_0/[PPEGMA]_0/[V\text{-}501]_0$ = 100:1:0.125 (molar ratio).

**RAFT Emulsion Polymerization of MMA, EMA, and PrMA with $PPEGMA_{19}$ Macro-CTA.** Using the $PPEGMA_{19}$ macro-CTA, three hydrophobic methacrylates, MMA, EMA, and PrMA, underwent RAFT emulsion polymerization (block copolymerization) with stirring at 600 rpm at 70 °C for 24 h. A series of block copolymers were synthesized with various target DPs (=$m$) of hydrophobic methacrylates in the range of 75−200. Considering the solubility of the monomer, emulsion polymerization proceeded in all of the polymerization conditions at 20 wt % solids conc. As a typical example, RAFT emulsion polymerization for $PPEGMA_{19}$-$b$-$PEMA_{100}$ is shown. Figure 1 shows MWDs by SEC with respect to the change in polymerization time. As the polymerization time increased, the MWD shifted to a higher molecular weight while maintaining a relatively narrow $M_w/M_n$ value. Polymerization continued for more than 5 h and was finally terminated at 24 h. Note that no dependence of morphology on polymerization time was found between 5 and 24 h (Figure S2 of the Supporting Information). It will take enough time for the polymerization to complete. BuMA with a low $T_g$, which will be described later, does not change in morphology at 6 and 24 h (Figure S2). However, in dispersion polymerization using an organic solvent with a high polymerization rate, there is an example in which the morphology changes after the polymerization is completed.[48]

Table 2 summarizes the results of typical RAFT-mediated emulsion polymerizations of MMA, EMA, and PrMA using the $PPEGMA_{19}$ macro-CTA (entries 1−9), as well as other polymerization results for BuMA (entries 13 and 14), ADMA (entries 15 and 16), and THFMA (entries 17 and 18). The resulting block copolymer morphologies via RAFT emulsion polymerization are also shown.

An aliquot of the as-quenched emulsion polymerization mixture was diluted with $D_2O$ and measured by $^1$H NMR spectroscopy. The remainder was diluted with a good solvent of either $d_4$-methanol or a $d_4$-methanol/$CDCl_3$ mixture until it became transparent and was measured by $^1$H NMR spectroscopy. Representative $^1$H NMR results for the emulsion polymerization of EMA are shown in Figure 2. In the case of entry 4, when the target DP of PEMA was 75 at full monomer

**Table 2. Representative Results of RAFT Emulsion Polymerization of Various Core-Forming Methacrylates at 70 °C Using PPEGMA Macro-CTA[a]**

| entry | structure[b] | target core DP | solids[c] (wt %) | convn[d] (%) | $M_{n,th}$[e] | $M_{n,SEC}$[f] | $M_w/M_n$[f] | $D_h$[g] (nm) | PDI[g] | morphology[h] |
|---|---|---|---|---|---|---|---|---|---|---|
| 1 | $PPEGMA_{19}$-$b$-$PMMA_{100}$ | 100 | 20 | >99 | 19 900 | 19 700 | 1.10 | 25 | 0.10 | S |
| 2 | $PPEGMA_{19}$-$b$-$PMMA_{150}$ | 150 | 20 | >99 | 24 800 | 22 500 | 1.10 | 44 | 0.61 | W |
| 3 | $PPEGMA_{19}$-$b$-$PMMA_{200}$ | 200 | 20 | >99 | 29 900 | 25 600 | 1.18 | 936 | 0.43 | W |
| 4 | $PPEGMA_{19}$-$b$-$PEMA_{75}$ | 75 | 20 | >99 | 18 400 | 18 800 | 1.11 | 17 | 0.47 | S (+W) |
| 5 | $PPEGMA_{19}$-$b$-$PEMA_{100}$ | 100 | 20 | >99 | 21 300 | 21 500 | 1.11 | 48 | 0.55 | W + T |
| 6 | $PPEGMA_{19}$-$b$-$PEMA_{148}$ | 150 | 20 | 99 | 26 900 | 27 700 | 1.13 | 629 | 0.35 | T + V |
| 7 | $PPEGMA_{19}$-$b$-$PPrMA_{75}$ | 75 | 20 | >99 | 19 500 | 18 100 | 1.12 | 71 | 0.40 | W + T |
| 8 | $PPEGMA_{19}$-$b$-$PPrMA_{99}$ | 100 | 20 | 99 | 22 700 | 25 600 | 1.07 | 55 | 0.14 | V (+W) |
| 9 | $PPEGMA_{19}$-$b$-$PPrMA_{148}$ | 150 | 20 | 99 | 28 900 | 30 200 | 1.15 | 83 | 0.14 | V |
| 10 | $PPEGMA_{10}$-$b$-$PEMA_{59}$ | 60 | 20 | 98 | 12 000 | 13 600 | 1.09 | 115 | 0.76 | W |
| 11 | $PPEGMA_{10}$-$b$-$PEMA_{94}$ | 96 | 20 | 97 | 16 100 | 19 600 | 1.13 | 828 | 0.22 | V |
| 12 | $PPEGMA_{29}$-$b$-$PEMA_{240}$ | 241 | 20 | 99 | 42 500 | 40 600 | 1.33 | 140 | 0.29 | S |
| 13 | $PPEGMA_{19}$-$b$-$PBuMA_{100}$ | 100 | 20 | >99 | 24 100 | 22 600 | 1.11 | 29 | 0.19 | S |
| 14 | $PPEGMA_{19}$-$b$-$PBuMA_{150}$ | 150 | 20 | >99 | 31 200 | 35 000 | 1.12 | 61 | 0.10 | V |
| 15 | $PPEGMA_{19}$-$b$-$PADMA_{60}$ | 75 | 20 | 80 | 23 100 | 18 600 | 1.34 | 878[i] | 0.42 | S |
| 16 | $PPEGMA_{19}$-$b$-$PADMA_{134}$ | 150 | 20 | 89 | 39 300 | 31 500 | 1.62 | 213[i] | 0.31 | S |
| 17 | $PPEGMA_{19}$-$b$-$PTHFMA_{74}$ | 75 | 20 | 99 | 22 600 | 19 500 | 1.09 | 978 | 0.55 | W |
| 18 | $PPEGMA_{19}$-$b$-$PTHFMA_{99}$ | 100 | 20 | 99 | 26 800 | 23 600 | 1.09 | 1224 | 0.50 | W |

[a] $[Monomer]_0/[PPEGMA]_0/[V\text{-}501]_0$ = 75−388:1:0.125 (molar ratio). All polymerizations were conducted for a day. The final assembly morphology did not change with continued heating after the polymerization has been completed. All of the final reaction mixtures were turbid, except for entries 1, 4, and 13. [b] DP of core block: target core DP × convn. [c] Solids concentration (wt %) = 100 × [PPEGMA macro-CTA (g) + monomer (g) + V-501 (g)]/[all reaction mixtures (g)]. [d] By monomer consumption using $^1$H NMR spectroscopy. [e] $M_{n,th}$ = $M_{n,PPEGMA\ macro\text{-}CTA}$ + target DP × $MW_{core\text{-}forming\ monomer}$ × convn. [f] By SEC in THF (PMMA standards). [g] By DLS measurement at 25 °C. [h] By dynamic-mode AFM analysis: S = spheres, W = worms, T = toroids, and V = vesicles. [i] Partly necklace-like spheres.



https://doi.org/10.1021/acsomega.2c03440
ACS Omega 2022, 7, 26894−26904

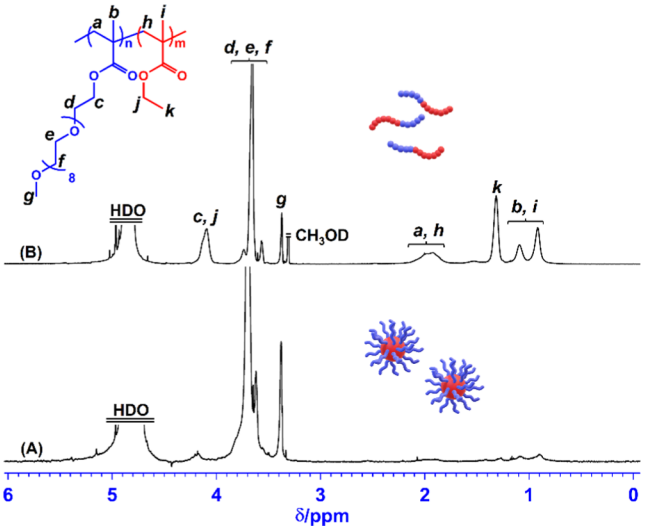


**Figure 2.** $^1$H NMR spectra at 20 °C of PPEGMA$_{19}$-*b*-PEMA$_{75}$ (entry 4) prepared from RAFT emulsion polymerization directly diluted with (A) $D_2O$ or (B) $d_4$-methanol.

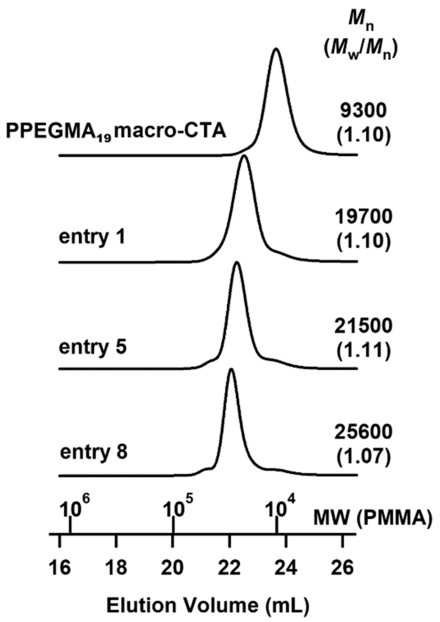


**Figure 3.** Typical SEC traces of the resultant of entries 1, 5, and 8.

conversion, only signals from the PPEGMA moiety are observed in the spectrum, and no (or only broad) PEMA signals are visible in $D_2O$ in Figure 2A. In contrast, all proton signals expected for the PPEGMA and PEMA chains are clearly visible in the $^1$H NMR spectrum recorded in $d_4$-methanol in Figure 2B. These $^1$H NMR observations suggest that the PPEGMA$_{19}$ chains act as the reactive emulsifier (shell), while the PEMA chains form the micelle core, as expected. Furthermore, since the characteristic methylene proton signals derived from the EMA monomer were not observed at 5.5−6.2 ppm, full monomer conversion is confirmed in this case. Thus, the resultant diblock copolymer composition was determined from the monomer conversion to be $n$ = 19 and $m$ = 75, i.e., PPEGMA$_{19}$-*b*-PEMA$_{75}$, assuming 100% blocking efficiency for the PPEGMA$_{19}$ macro-CTA. The composition was also confirmed from the area ratio of peaks (c and k) in Figure 2B. All of the synthesized block copolymer compositions were determined similarly, as shown in entries 1−18 of Table 2.

Figure 3 shows typical SEC curves for entries 1, 5, and 8. These results correspond to those for block copolymers via RAFT emulsion polymerization of MMA, EMA, and PrMA, respectively, with a target DP = 100 using a PPEGMA$_{19}$ macro-CTA. Thus, $[PPEGMA_{19}]_0/[\text{hydrophobic methacrylate}]_0$ was set to a molar ratio of 100. All polymers have a nearly monodisperse distribution with a narrow MWD ($M_w/M_n$ = 1.07−1.11). The high- and low-molecular-weight regions have very slight shoulders. These are likely due to polymers via termination such as combination and residual PPEGMA homopolymers that do not act as macro-CTAs, respectively. However, the MWD is shifted toward a significantly higher molecular weight relative to the PPEGMA$_{19}$ macro-CTA, depending on the molecular weight of the hydrophobic methacrylate, i.e., MMA < EMA < PrMA. Each $M_n$ is in good agreement with the target DP in the conversion. Similarly, irrespective of the target DP of the core poly(methacrylate) and PPEGMA macro-CTA length ($n$ = 10−29), similar block copolymers with narrow MWDs ($M_w/M_n$ = 1.07−1.18) were obtained via RAFT emulsion polymerization of the three hydrophobic methacrylates in entries 1−12 of Table 2.

AFM studies confirmed that these RAFT emulsion formulations provided higher-order morphologies, depending on the composition of the resultant block copolymer. Figure 4 shows AFM images of the morphological changes with respect to the DP of the core-forming poly(methacrylate). The cores of PMMA, PEMA, and PPrMA are arranged vertically, and the horizontal axis is the target DP of the core. The conversions for entries 1−9 shown here were greater than 98%. Even in cores such as PMMA, where $T_g$ is higher than the polymerization temperature, which is disadvantageous for morphological transition, morphological changes from spheres occurred. It is also possible that the monomer acts as a plasticizer.[49] The shorter the chain length, the lower the $T_g$ of PMMA.[50] Thus, short-chain PMMA has sufficient mobility at the polymerization temperature and may cause morphological changes. However, since DPs of PMMAs are 150 and 200 for entries 2 and 3, respectively, and the $T_g$ of final products is significantly above the polymerization temperature. Hence, this is likely due to the high solubility of the monomer in water. In the range from entries 1−3, no morphological change from worms to vesicles was found. This is because the worms could not transform to vesicles at longer chain lengths due to the higher $T_g$ of the core block as the DP of PMMA increased.

Herein, we focused on emulsion polymerization of alkyl methactylates using PPEGMA macro-CTA, but only spheres were obtained with a different shell of PGMA macro-CTA.[51] In addition, as described in the introduction, there is an example of morphological change using PDEGV macro-CTA with a high HLB value.[37] Thus, it is suggested that the mobility of the core-forming block stabilized by a shell during polymerization is a significant factor for morphology change at the temperature of RAFT emulsion polymerization. In practice, PrMA has relatively low solubility in water, but $T_g$ for PPrMA was sufficiently lower than the polymerization temperature. Thus, morphological change from worms (some toroids) to vesicles was observed (entries 7−9). Although the emulsion polymerization system is not homogeneous from the beginning, unlike at the start of dispersion polymerization, such morphological changes can occur. Even if either the solubility of the core-forming monomer


https://doi.org/10.1021/acsomega.2c03440
ACS Omega 2022, 7, 26894−26904

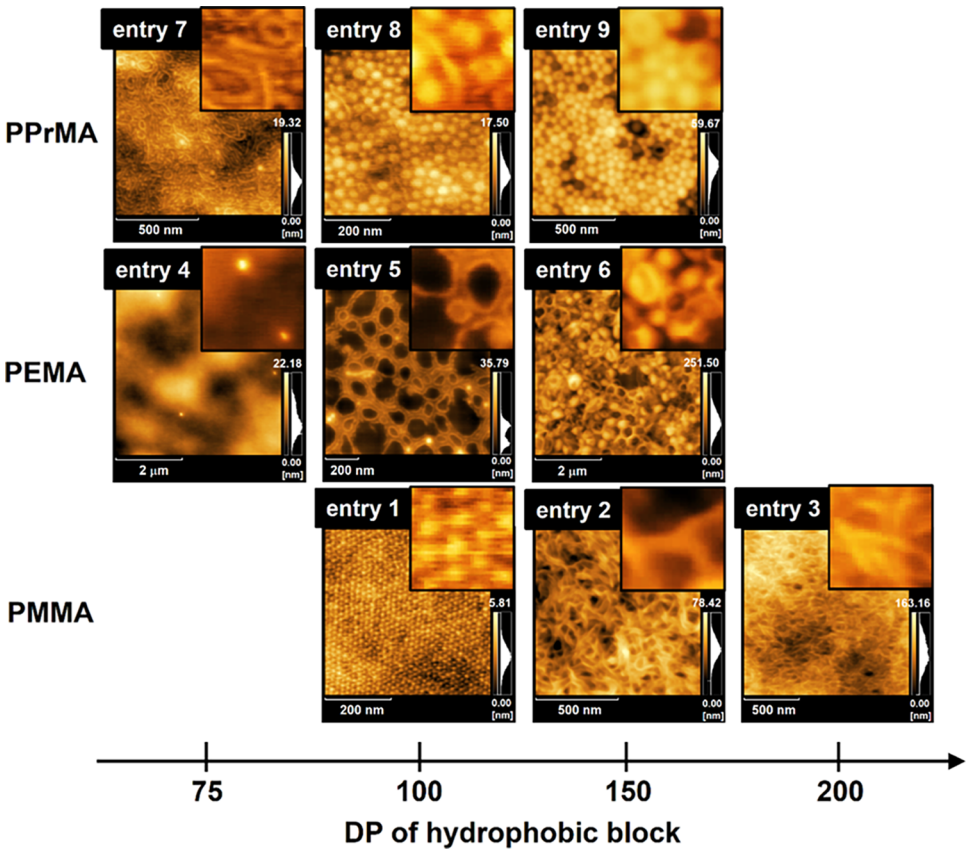


**Figure 4.** Representative AFM (height) images of nanoparticles prepared with a different target DP of hydrophobic core-forming block via RAFT emulsion polymerization of either MMA, EMA, or PrMA using the $PPEGMA_{19}$ macro-CTA at a solids concentration of 20 wt % at 70 °C: 500 × 500 $nm^2$ images for entries 1 and 8; 1 × 1 $\mu m^2$ images for entries 2, 5, 7; 1.5 × 1.5 $\mu m^2$ image for entry 3; and 5 × 5 $\mu m^2$ images for entries 4 and 6. Scale for the inset of magnified AFM images: 50 × 50 $nm^2$ for entry 1; 100 × 100 $nm^2$ for entries 2 and 8; 200 × 200 $nm^2$ for entries 3, 5, and 9; 1 × 1 $\mu m^2$ for entries 4 and 6; and 150 × 150 $nm^2$ for entry 7.

or $T_g$ for the core-forming block is an unfavorable condition, the possibility of morphological change has been found. In addition, when each DP for PEMA and PMMA was further increased (target DP of core-forming block > 250), a bimodal distribution in SEC was obtained (Figure S3). This is likely because the monomer could not diffuse into the micelle from the monomer droplet due to the influence of the high $T_g$ in the core-forming block, and higher molecular weight polymer formation occurred on the outside of the micelle. For the sample with DP = 100, viewed vertically in Figure 4, there was a difference in structure (spheres, worms/toroids, and vesicles for PMMA, PEMA, and PPrMA, respectively), even for the same DP. This is due to the systematic change in the packing parameter due to the volume change of the hydrophobic block. Therefore, these results suggest that the properties of the core that determine whether a morphological change occurs from spheres are a balance of three factors: (i) the solubility of the core-forming monomer in water, (ii) $T_g$ for the core-forming block relative to the polymerization temperature, and (iii) the hydrophobic core volume, which changes the packing parameter.

**Phase Diagram of PPEGMA-*b*-PEMA Prepared via RAFT Emulsion Polymerization.** Varying the target DP of the PEMA using a $PPEGMA_{10}$ or a $PPEGMA_{29}$ macro-CTA partly leads to similar morphological control. The morphological observations are summarized in the phase diagram shown in Figure 5. In the case of emulsion polymerization using $PPEGMA_{10}$, nearly monodisperse SEC curves were obtained (e.g., entry 10; Figure S4). The resulting nanoparticles were spheres, worms, and vesicles, depending on the DP of PEMA. When using $PPEGMA_{29}$, it was found that as the DP of PEMA was increased, the SEC curve became bimodal and higher molecular weights were obtained at DP > 241 in entry 12 (SEC curves; Figure S5). Judging from the packing parameter, due to the longer hydrophilic PPEGMA block, a sufficient length of the hydrophobic PEMA of the core-forming block is required for morphological change. However, morphological change cannot be seen in the region of $PPEGMA_{29}$. This is because of the difficulty of diffusion of EMA due to the high $T_g$ in the core-forming block, similar to that for the target $PPEGMA_{19}$-*b*-$PEMA_{300}$ and $PPEGMA_{19}$-*b*-$PMMA_{300}$ described above. Thus, morphological change cannot be seen in the region of $PPEGMA_{29}$. In the $PPEGMA_{29}$ series, only spheres were observed (AFM images; entry 12 in Figure 5 and others in Figure S6). In the case of such incomplete polymerization, a few worms and vesicles were sometimes observed. However, the morphology lacks reproducibility due to the presence of high-molecular-weight polymers. In the range where monomodal MWDs were obtained by SEC, spheres, worms, or vesicles were formed according to the DP of PEMA. This is due to the systematic change of the packing parameter due to the volume of the hydrophobic block. Worms were formed in the range where the DP was approximately PPEGMA/PEMA = 1:5, and vesicles were formed when the PEMA in the hydrophobic block was longer than that.

Next, BuMA, which has a lower $T_g$ for the homopolymer and a lower solubility in water than those for PrMA, was emulsion-


https://doi.org/10.1021/acsomega.2c03440
ACS Omega 2022, 7, 26894−26904

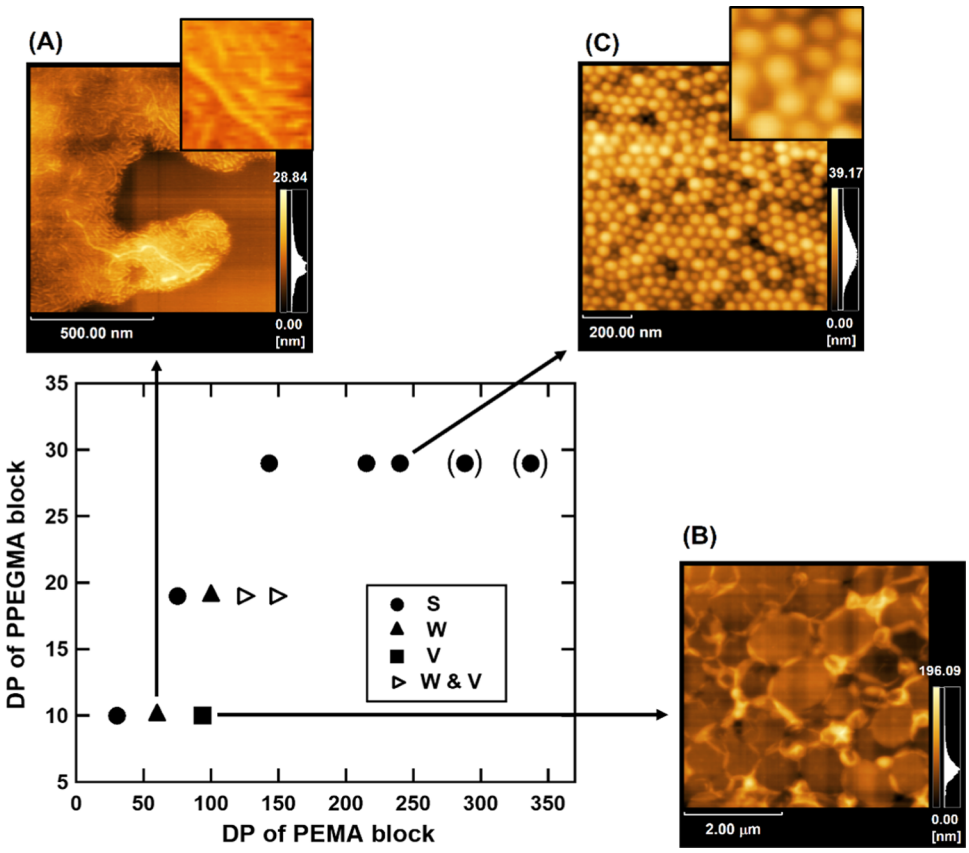


**Figure 5.** Phase diagram constructed for PPEGMA-*b*-PEMA nanoparticles: S = spheres, W = worms, and V = vesicles. Coexisting phases are indicated by two letters, where appropriate. Height AFM images for representative morphologies: (A) entry 10 [worms, 1 × 1 $\mu m^2$ image and scale bar = 500 nm (inset: magnified 125 × 125 $nm^2$ image)], (B) entry 11 [vesicles, 5 × 5 $\mu m^2$ image and scale bar = 2 $\mu m$], and (C) entry 12 [spheres, 1 × 1 $\mu m^2$ image and scale bar = 200 nm (inset: magnified 200 × 200 $nm^2$ image)]. Two black circles in parentheses are nanoparticles with a bimodal distribution in SEC.

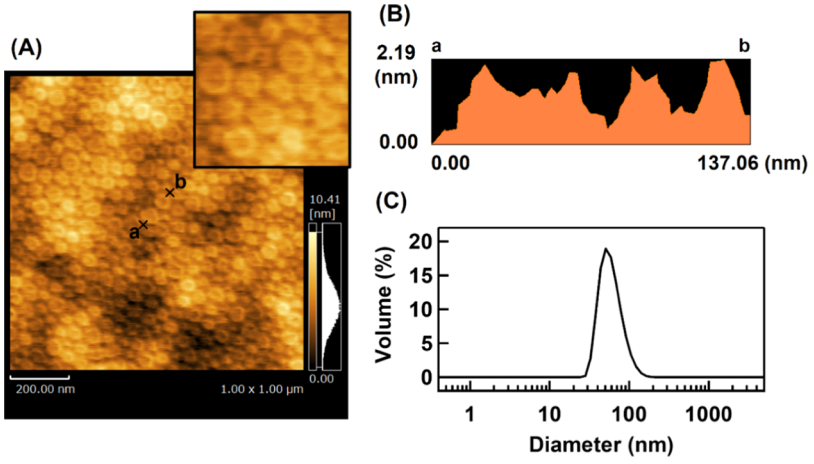


**Figure 6.** (A) AFM height images for entry 14 [vesicles, 1 × 1 $\mu m^2$ image and scale bar = 200 nm (inset: magnified 200 × 200 $nm^2$ image)], (B) a cross-sectional profile of a−b, and (C) DLS particle size distribution for the resultant vesicles in water.

polymerized using a $PPEGMA_{19}$ macro-CTA under the same conditions at 70 °C for 24 h at 20 wt % solid concentration: $[macro\text{-}CTA]_0/[EMA]_0/[V\text{-}501]_0$ = 1:100:0.125 or 1:150:0.125 (molar ratio). Polymerization proceeded smoothly, and well-defined block copolymers such as $PPEGMA_{19}$-*b*-$PBuMA_{100}$ and $PPEGMA_{19}$-*b*-$PBuMA_{150}$ were obtained. The polymerization results are shown in entries 13 and 14 in Table 2 (SEC curves; Figure S7). For entry 14, vesicles were observed in the AFM image, and a monomodal distribution was found by DLS analysis, as shown in Figure 6. Although $PPEGMA_{19}$-*b*-$PBuMA_{100}$ (entry 13) formed spheres (AFM image; Figure S8), $PPEGMA_{19}$-*b*-$PBuMA_{150}$ formed vesicles whose morphology was judged from the height of the central domain to be much lower than that at the edge (Figure 6B). Moreover, the mean diameter is smaller (61 nm) than any other polymer vesicles, and the PDI is relatively narrow (PDI = 0.10). Since PBuMA has the


https://doi.org/10.1021/acsomega.2c03440
ACS Omega 2022, 7, 26894−26904

highest volume among the use poly(alkyl methacrylate)s, the packing parameter for vesicle formation can be satisfied even if the DP of the core is the smallest among the methacrylates used in the present study. In fact, it is less soluble in water than PrMA, which is disadvantageous for morphology change. However, vesicles can be observed, since the $T_g$ for PBuMA is lower (20 °C) than the polymerization temperature (70 °C), and the chain mobility during polymerization is high. This morphological change may be caused primarily by the kinetically untrapped spheres under the polymerization conditions. However, the shorter PPEGMA$_{19}$-*b*-PBuMA$_{100}$ (entry 13) shows a spherical morphology, as expected. To the best of our knowledge, there have been no reports of morphological changes in RAFT emulsion polymerization of BuMA.[32] Various nanoparticles can be obtained through our comprehensive and systematic studies.

**Morphological Changes in Block Copolymers with Other Core Structures.** Based on the results so far, we investigated morphological changes in other core-forming methacrylates that differ from alkyl methacrylates, as shown in Table 3. Here, we used ADMA, which was expected from the packing parameter to easily change morphology because PADMA has a bulky side chain. However, the $T_g$ for PADMA is much higher than the polymerization temperature of 70 °C. Moreover, ADMA is a highly hydrophobic monomer with extremely low solubility in water. Thus, both $T_g$ and the monomer solubility in water are expected to work against a morphology change.

**Table 3. Properties of Core-Forming Block**[a]

| core-forming block | PTHFMA | PADMA |
|---|---|---|
| $T_g$ (°C) | 57 | 202 |
| soly. of monomer (g/L)[b,c] | 6.0 | 0.026 |

[a]Refs 52 and 53. [b]Aqueous solubility at 25 °C. [c]Calculated data from Advanced Chemistry Development (ACD/Labs).

RAFT emulsion polymerization of ADMA was conducted at target DPs of PADMA = 75 and 150, affording nanoparticles of PPEGMA$_{19}$-*b*-PADMA$_{60}$ (entry 15) and PPEGMA$_{19}$-*b*-PADMA$_{134}$ (entry 16) in situ. These polymerizations had broader MWDs than other entries in Table 2 (SEC curves; Figure S9). In particular, the larger the DP of the target PADMA, the broader the MWD. This is likely due to the highly hydrophobic ADMA and high $T_g$ for PADMA. Figure 7 shows AFM images of nonmorphological changes with respect to the DP of core-forming PADMA. Despite the increase in the DP of PADMA from 60 to 134, the spherical shape was maintained, and the mean diameter in the AFM image increased from 33 to 63 nm, even in a dry state. Interestingly, physical gelation was observed visually for both entries 15 and 16 during polymerization at a solid concentration of 20 wt %. However, the gelation was not due to the entanglement of worms. Since the mean diameters by DLS analysis in Table 2 are obviously larger than those in the AFM images, the resulting spheres are likely to form a macrolattice by collisions between spheres.[54] This indicates that the spheres are simply connected to each other while maintaining their shape. Since $T_g$ for PADMA is too high, the core mobility is poor during polymerization. Since collisions between spheres can transform spheres into worms,[24] it would be necessary to devise a shell structure for PADMA in the future.

We next investigated RAFT emulsion polymerization of THFMA using the same PPEGMA$_{19}$ macro-CTA. THFMA has intermediate physical properties (solubility of monomer in water and $T_g$ of the polymer) between those for EMA and PrMA. Therefore, it is expected that morphologies other than spheres can be easily created. When polymerization was conducted at target DPs of PTHFMA = 75 and 100, nanoparticles of PPEGMA$_{19}$-*b*-PTHFMA$_{74}$ (entry 17) and PPEGMA$_{19}$-*b*-PTHFMA$_{99}$ (entry 18) were obtained in situ. Both polymerization mixtures were physically gelled during the polymerization process, but well-defined block copolymers with narrow MWDs ($M_w/M_n$ < 1.1) were obtained at almost full conversions in 24 h (SEC curves; Figure S10). Figure 8 shows AFM images of the resulting nanoparticles for entries 17 and 18. As expected, both possessed worm-like morphologies that differed from spheres. In particular, the longer the chain length of PTHFMA, the larger the worm diameter. This is the result of the morphology control using Figures 4 and 5 as a road map for various nanoparticles. Therefore, if the solubility of the core-forming monomer in water and $T_g$ for the polymer are similar to those for EMA and PrMA, the morphology can be controlled via RAFT emulsion polymerization using PPEGMA macro-CTA at 70 °C.

**Stable Worms of Crosslinked PPEGMA-*b*-PEMA Using EGDMA.** Stable nanoparticles with a crosslinked core were prepared as a typical example. The worms derived from PPEGMA$_{19}$-*b*-PEMA$_{100}$ synthesized by RAFT emulsion polymerization (entry 5) have a frozen structure in water and do not change even when diluted with water. However, when dissolved in ethanol or chloroform as good solvents for both segments, the

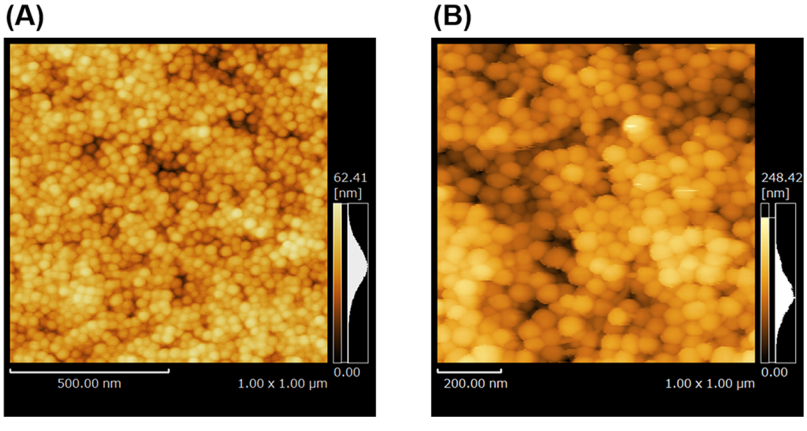


**Figure 7.** AFM height images for (A) entry 15 and (B) entry 16 [spheres; 1 × 1 $\mu m^2$ images].



https://doi.org/10.1021/acsomega.2c03440
ACS Omega 2022, 7, 26894−26904

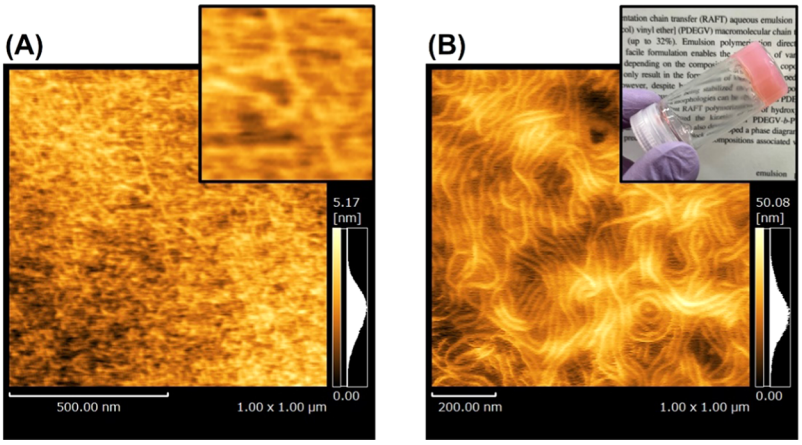


**Figure 8.** AFM height images for (A) entry 17 [worms; 1 × 1 $\mu m^2$ images, (inset: magnified 200 × 200 $nm^2$ image)] and (B) entry 18 [worms; 1 × 1 $\mu m^2$ images, (inset: digital photograph obtained for the inclined sample tube after emulsion polymerization)].

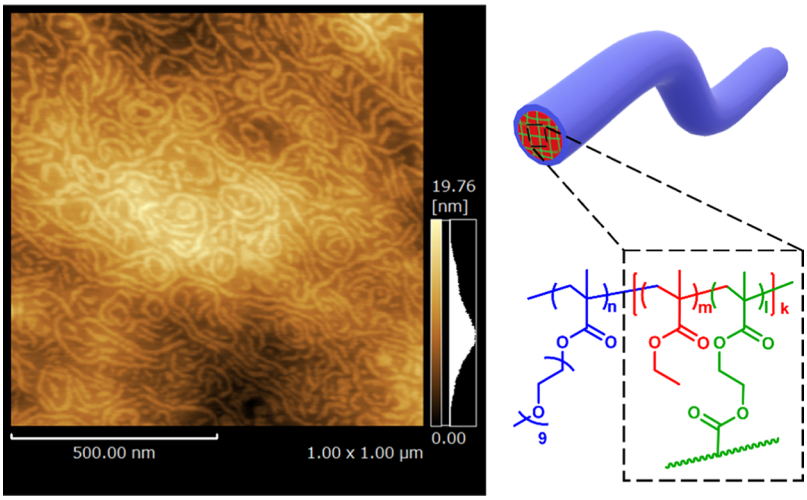


**Figure 9.** AFM height image for stable crosslinked worms derived from $PPEGMA_{19}$-*b*-$PEMA_{100}$ (entry 5) [1 × 1 $\mu m^2$ image]. The target structure is shown as $PPEGMA_{19}$-*b*-$P(EMA_{0.98}$-*co*-$EGDMA_{0.02})_{102}$ on the basis of polymerization condition.

worms dissolve because they are physical aggregates of micelles. Thus, RAFT emulsion polymerization was performed by adding 2 mol % EGDMA during PEMA polymerization so that $PPEGMA_{19}$-*b*-$PEMA_{100}$ could withstand solvent changes, and the core was crosslinked to obtain stable worms. Ethanol was added to the aqueous solution of the resulting nanoparticles obtained after emulsion polymerization, and the same amount of chloroform was added until it became transparent. Figure 9 shows an AFM image of nanoparticles in the crosslinked $PPEGMA_{19}$-*b*-$PEMA_{100}$, i.e., $PPEGMA_{19}$-*b*-$P(EMA_{0.98}$-*co*-$EGDMA_{0.02})_{102}$. It can be seen that the worm shape is maintained even in an ethanol/chloroform mixture. Although $PPEGMA_{19}$-*b*-$PEMA_{100}$ obtained via RAFT emulsion polymerization (entry 5) was completely dissolved in an ethanol/chloroform mixture by the same operation, the crosslinked $PPEGMA_{19}$-*b*-$PEMA_{100}$ worms remained intact. Therefore, it is possible to obtain stable worms in situ by RAFT emulsion polymerization.

## CONCLUSIONS

RAFT emulsion polymerization of alkyl methacrylates such as MMA, EMA, and PrMA at 70 °C using PPEGMA macro-CTA was conducted for the formation of nanoparticles with shapes such as spheres, worms (toroids), and vesicles. We found that higher-order morphologies could be obtained by increasing the DP of the core and the alkyl chain length in the pendant of the core. Thus, the systematic change of morphology due to increasing volume of the hydrophobic block was confirmed. Even in cores such as PMMA, where $T_g$ is higher than the polymerization temperature, which is disadvantageous for morphological transition, morphological changes from spheres occurred. This is due to the high solubility of the monomer in water. However, when PMMA was used for the core, no morphological change from worms to vesicles occurred. This is because the worms could not transform to vesicles at longer chain lengths due to the higher $T_g$ of the core block as DP increased. On the basis of these morphology changes, the main properties of the core that determine whether morphological change occurs from spheres were the balance of three factors: (i) the solubility of the core-forming monomer in water, (ii) $T_g$ for the core-forming block relative to the polymerization temperature, and (iii) the hydrophobic core volume, which changes the packing parameter. Knowledge of these factors enabled the prediction of morphology changes by RAFT emulsion polymerization of methacrylates using PPEGMA macro-CTA. The resulting PBuMA vesicles were observed despite the lower solubility of the core-forming monomer in water. In the case of ADMA, which has the highest $T_g$ core-forming block and lowest


https://doi.org/10.1021/acsomega.2c03440
ACS Omega 2022, 7, 26894−26904

aqueous solubility, spherical particles were maintained in spite of the bulky side chain, as expected. THFMA has intermediate physical properties (solubility of monomer in water and $T_g$ for the polymer) between EMA and PrMA. Therefore, morphologies other than spheres were easily produced. Finally, RAFT emulsion polymerization was performed in the presence of a cross-linking agent (2 mol % EGDMA) to prepare PPEGMA$_{19}$-*b*-P(EMA$_{0.98}$-*co*-EGDMA$_{0.02}$)$_{102}$ worms that remained intact in the presence of a good solvent for both blocks.

## ■ ASSOCIATED CONTENT

### Supporting Information

The Supporting Information is available free of charge at https://pubs.acs.org/doi/10.1021/acsomega.2c03440.

$^1$H NMR spectra of PPEGMA macro-CTA; AFM (height) images for the resulting nanoparticles; SEC curves for targeted PPEGMA$_{19}$-*b*-PEMA$_{300}$, targeted PPEGMA$_{19}$-*b*-PMMA$_{300}$, entry 10, targeted PPEGMA$_{29}$-*b*-PEMA$_m$, and entries 13−18 (PDF)

## ■ AUTHOR INFORMATION


### Corresponding Author

**Shinji Sugihara** − *Department of Applied Chemistry and Biotechnology, Graduate School of Engineering, University of Fukui, Fukui 910-8507, Japan;* orcid.org/0000-0002-7091-3994; Email: sugihara@u-fukui.ac.jp

### Authors

**Atsushi Takashima** − *Department of Applied Chemistry and Biotechnology, Graduate School of Engineering, University of Fukui, Fukui 910-8507, Japan*

**Yasushi Maeda** − *Department of Applied Chemistry and Biotechnology, Graduate School of Engineering, University of Fukui, Fukui 910-8507, Japan*

Complete contact information is available at: https://pubs.acs.org/10.1021/acsomega.2c03440


### Author Contributions

A.T.: Data curation, experiments, analysis, and writing—original draft. Y.M.: data curation and investigation. S.S.: conceptualization, methodology, investigation, validation, supervision, funding acquisition, writing—original draft, reviewing, and editing.

### Notes

The authors declare no competing financial interest.

## ■ ACKNOWLEDGMENTS

We thank Osaka Organic Chemical Industry, Ltd., for kindly supplying ADMA. This work was partially supported by JSPS KAKENHI Grant Number 19H02762.

## ■ REFERENCES


(1) Sugihara, S. In *Molecular Technology, Volume 4: Synthesis Innovation*Yamamoto, H.; Kato, T., Eds.; Wiley-VCH: Weinheim, 2019; Vol. 4, pp 1−29.

(2) Wang, X.; An, Z. New Insights into RAFT Dispersion Polymerization-Induced Self-Assembly: from Monomer Library, Morphological Control, and Stability to Driving Forces. *Macromol. Rapid Commun.* **2019**, *40*, No. 1800325.

(3) Derry, M. J.; Fielding, L. A.; Armes, S. P. Polymerization-induced self-assembly of block copolymer nanoparticles via RAFT non-aqueous dispersion polymerization. *Prog. Polym. Sci.* **2016**, *52*, 1−18.

(4) Canning, S. L.; Smith, G. N.; Armes, S. P. A Critical Appraisal of RAFT-Mediated Polymerization-Induced Self-Assembly. *Macromolecules* **2016**, *49*, 1985−2001.

(5) Lowe, A. B. RAFT alcoholic dispersion polymerization with polymerization-induced self-assembly. *Polymer* **2016**, *106*, 161−181.

(6) Warren, N. J.; Armes, S. P. Polymerization-Induced Self-assembly of Block Copolymer Nano-objects via RAFT Aqueous Dispersion Polymerization. *J. Am. Chem. Soc.* **2014**, *136*, 10174−10185.

(7) Sun, J. T.; Hong, C.-Y.; Pan, C. Y. Recent advances in RAFT dispersion polymerization for preparation of block copolymer aggregates. *Polym. Chem.* **2013**, *4*, 873−881.

(8) Charleux, B.; Delaittre, G.; Rieger, J.; D'Agosto, F. Polymerization-Induced Self-Assembly: From Soluble Macromolecules to Block Copolymer Nano-Objects in One Step. *Macromolecules* **2012**, *45*, 6753−6765.

(9) D'Agosto, F.; Rieger, J.; Lansalot, M. RAFT-Mediated Polymerization-Induced Self-Assembly. *Angew. Chem., Int. Ed.* **2020**, *59*, 8368−8392.

(10) Mai, Y.; Eisenberg, A. Self-assembly of block copolymers. *Chem. Soc. Rev.* **2012**, *41*, 5969−5985.

(11) Chiefari, J.; Chong, Y. K.; Ercole, F.; Krstina, J.; Jeffery, J.; Le, T. P. T.; Mayadunne, R. T. A.; Meijs, G. F.; Moad, C. L.; Moad, G.; Rizzardo, E.; Thang, S. H. Living Free-Radical Polymerization by Reversible Addition−Fragmentation Chain Transfer: The RAFT Process. *Macromolecules* **1998**, *31*, 5559−5562.

(12) Moad, G.; Rizzardo, E.; Thang, S. H. Living Radical Polymerization by the RAFT Process A Third Update. *Aust. J. Chem.* **2012**, *65*, 985−1076.

(13) Israelachvili, J. N.*Intermolecular and Surface Forces*; Academic Press: London, 1991.

(14) Antonietti, M.; Förster, S. Vesicles and Liposomes: A Self-Assembly Principle Beyond Lipids. *Adv. Mater.* **2003**, *15*, 1323−1333.

(15) Sugihara, S.; Sugihara, K.; Armes, S. P.; Ahmad, H.; Lewis, A. L. Synthesis of Biomimetic Poly(2-(methacryloyloxy)ethyl phosphorylcholine) Nanolatexes via Atom Transfer Radical Dispersion Polymerization in Alcohol/Water Mixtures. *Macromolecules* **2010**, *43*, 6321−6329.

(16) Sugihara, S.; Armes, S. P.; Lewis, A. L. One-Pot Synthesis of Biomimetic Shell Cross-Linked Micelles and Nanocages by ATRP in Alcohol/Water Mixtures. *Angew. Chem., Int. Ed.* **2010**, *49*, 3500−3503.

(17) Sugihara, S.; Ma'Radzi, A. H.; Ida, S.; Irie, S.; Kikukawa, T.; Maeda, Y. In situ nano-objects via RAFT aqueous dispersion polymerization of 2-methoxyethyl acrylate using poly(ethylene oxide) macromolecular chain transfer agent as steric stabilizer. *Polymer* **2015**, *76*, 17−24.

(18) Sugihara, S.; Blanazs, A.; Armes, S. P.; Ryan, A. J.; Lewis, A. L. Aqueous Dispersion Polymerization: A New Paradigm for in Situ Block Copolymer Self-Assembly in Concentrated Solution. *J. Am. Chem. Soc.* **2011**, *133*, 15707−15713.

(19) Sugihara, S.; Armes, S. P.; Blanazs, A.; Lewis, A. L. Non-spherical morphologies from cross-linked biomimetic diblock copolymers using RAFT aqueous dispersion polymerization. *Soft Matter* **2011**, *7*, 10787−10793.

(20) Fielding, L. A.; Derry, M. J.; Ladmiral, V.; Rosselgong, J.; Rodrigues, A. M.; Ratcliffe, L. P. D.; Sugihara, S.; Armes, S. P. RAFT dispersion polymerization in non-polar solvents: facile production of block copolymer spheres, worms and vesicles in *n*-alkanes. *Chem. Sci.* **2013**, *4*, 2081−2087.

(21) Sugihara, S.; Sudo, M.; Maeda, Y. Synthesis and Nano-object Assembly of Biomimetic Block Copolymers for Catalytic Silver Nanoparticles. *Langmuir* **2019**, *35*, 1346−1356.

(22) Blanazs, A.; Ryan, A. J.; Armes, S. P. Predictive Phase Diagrams for RAFT Aqueous Dispersion Polymerization: Effect of Block Copolymer Composition, Molecular Weight, and Copolymer Concentration. *Macromolecules* **2012**, *45*, 5099−5107.

(23) Blanazs, A.; Verber, R.; Mykhaylyk, O. O.; Ryan, A. J.; Heath, J. Z.; Douglas, C. W. I.; Armes, S. P. Sterilizable Gels from Thermoresponsive Block Copolymer Worms. *J. Am. Chem. Soc.* **2012**, *134*, 9741−9748.

(24) Tan, J.; Sun, H.; Yu, M.; Sumerlin, B. S.; Zhang, L. Photo-PISA: Shedding Light on Polymerization-Induced Self-Assembly. *ACS Macro Lett.* **2015**, *4*, 1249−1253.
(25) Figg, C. A.; Simula, A.; Gebre, K. A.; Tucker, B. S.; Haddleton, D. M.; Sumerlin, B. S. Polymerization-induced thermal self-assembly (PITSA). *Chem. Sci.* **2015**, *6*, 1230−1236.
(26) Karagoz, B.; Esser, L.; Duong, H. T.; Basuki, J. S.; Boyer, C.; Davis, T. P. Polymerization-Induced Self-Assembly (PISA) − control over the morphology of nanoparticles for drug delivery applications. *Polym. Chem.* **2014**, *5*, 350−355.
(27) Boissé, S.; Rieger, J.; Belal, K.; Di-Cicco, A.; Beaunier, P.; Li, M. H.; Charleux, B. Amphiphilic block copolymer nano-fibers via RAFT-mediated polymerization in aqueous dispersed system. *Chem. Commun.* **2010**, *46*, 1950−1952.
(28) Zhang, X.; Boisse, S.; Zhang, W.; Beaunier, P.; D'Agosto, F.; Rieger, J.; Charleux, B. Well-Defined Amphiphilic Block Copolymers and Nano-objects Formed *In Situ* via RAFT-Mediated Aqueous Emulsion Polymerization. *Macromolecules* **2011**, *44*, 4149−4158.
(29) Boissé, S.; Rieger, J.; Pembouong, G.; Beaunier, P.; Charleux, B. Influence of the stirring speed and $CaCl_2$ concentration on the nano-object morphologies obtained via RAFT-mediated aqueous emulsion polymerization in the presence of a water-soluble macroRAFT agent. *J. Polym. Sci., Part A: Polym. Chem.* **2011**, *49*, 3346−3354.
(30) Zhang, W.; D'Agosto, F.; Boyron, O.; Rieger, J.; Charleux, B. Toward a Better Understanding of the Parameters that Lead to the Formation of Nonspherical Polystyrene Particles via RAFT-Mediated One-Pot Aqueous Emulsion Polymerization. *Macromolecules* **2012**, *45*, 4075−4084.
(31) Khor, S. Y.; Truong, N. P.; Quinn, J. F.; Whittaker, M. R.; Davis, T. P. Polymerization-Induced Self-Assembly: The Effect of End Group and Initiator Concentration on Morphology of Nanoparticles Prepared via RAFT Aqueous Emulsion Polymerization. *ACS Macro Lett.* **2017**, *6*, 1013−1019.
(32) Truong, N. P.; Quinn, J. F.; Anastasaki, A.; Haddleton, D. M.; Whittaker, M. R.; Davis, T. P. Facile access to thermoresponsive filomicelles with tuneable cores. *Chem. Commun.* **2016**, *52*, 4497−4500.
(33) Truong, N. P.; Whittaker, M. R.; Anastasaki, A.; Haddleton, D. M.; Quinn, J. F.; Davis, T. P. Facile production of nanoaggregates with tuneable morphologies from thermoresponsive P(DEGMA-*co*-HPMA). *Polym. Chem.* **2016**, *7*, 430−440.
(34) Truong, N. P.; Quinn, J. F.; Anastasaki, A.; Rolland, M.; Vu, M. N.; Haddleton, D. M.; Whittaker, M. R.; Davis, T. P. Surfactant-free RAFT emulsion polymerization using a novel biocompatible thermoresponsive polymer. *Polym. Chem.* **2017**, *8*, 1353−1363.
(35) Lesage de la Haye, J.; Zhang, X.; Chaduc, I.; Brunel, F.; Lansalot, M.; D'Agosto, F. The Effect of Hydrophile Topology in RAFT-Mediated Polymerization-Induced Self-Assembly. *Angew. Chem., Int. Ed.* **2016**, *55*, 3739−3743.
(36) Brunel, F.; de la Haye, J. L.; Lansalot, M.; D'Agosto, F. New Insight into Cluster Aggregation Mechanism during Polymerization-Induced Self-Assembly by Molecular Dynamics Simulation. *J. Phys. Chem. B* **2019**, *123*, 6609−6617.
(37) Sugihara, S.; Kawakami, R.; Irie, S.; Maeda, Y. Poly[di(ethylene glycol) vinyl ether]-stabilized poly(vinyl acetate) nanoparticles with various morphologies via RAFT aqueous emulsion polymerization of vinyl acetate. *Polym. J.* **2021**, *53*, 309−321.
(38) Brotherton, E. E.; Hatton, F. L.; Cockram, A. A.; Derry, M. J.; Czajka, A.; Cornel, E. J.; Topham, P. D.; Mykhaylyk, O. O.; Armes, S. P. In Situ Small-Angle X-ray Scattering Studies During Reversible Addition−Fragmentation Chain Transfer Aqueous Emulsion Polymerization. *J. Am. Chem. Soc.* **2019**, *141*, 13664−13675.
(39) Cockram, A. A.; Neal, T. J.; Derry, M. J.; Mykhaylyk, O. O.; Williams, N. S. J.; Murray, M. W.; Emmett, S. N.; Armes, S. P. Effect of Monomer Solubility on the Evolution of Copolymer Morphology during Polymerization-Induced Self-Assembly in Aqueous Solution. *Macromolecules* **2017**, *50*, 796−802.
(40) Man, S. K.; Wang, X.; Zheng, J. W.; An, Z. S. Effect of Butyl α-Hydroxymethyl Acrylate Monomer Structure on the Morphology Produced via Aqueous Emulsion Polymerization-induced Self-assembly. *Chin. J. Polym. Sci.* **2020**, *38*, 9−16.
(41) Hatton, F. L.; Park, A. M.; Zhang, Y.; Fuchs, G. D.; Ober, C. K.; Armes, S. P. Aqueous One-Pot Synthesis of Epoxy-Functional Diblock Copolymer Worms from a Single Monomer: New Anisotropic Scaffolds for Potential Charge Storage Applications. *Polym. Chem.* **2019**, *10*, 194−200.
(42) Hatton, F. L.; Derry, M. J.; Armes, S. P. Rational synthesis of epoxy-functional spheres, worms and vesicles by RAFT aqueous emulsion polymerisation of glycidyl methacrylate. *Polym. Chem.* **2020**, *11*, 6343−6355.
(43) Dai, X.; Yu, L.; Zhang, Y.; Zhang, L.; Tan, J. Polymerization-Induced Self-Assembly via RAFT-Mediated Emulsion Polymerization of Methacrylic Monomers. *Macromolecules* **2019**, *52*, 7468−7476.
(44) Schneider, H. A. Polymer class specificity of the glass temperature. *Polymer* **2005**, *46*, 2230−2237.
(45) Chai, X.-S.; Schork, F. J.; DeCinque, A.; Wilson, K. Measurement of the Solubilities of Vinylic Monomers in Water. *Ind. Eng. Chem. Res.* **2005**, *44*, 5256−5258.
(46) Penzel, E.*Ullmann's Encyclopedia of Industrial Chemistry*, 7th ed.; Wiley-VCH, 2008.
(47) Mitsukami, Y.; Donovan, M. S.; Lowe, A. B.; McCormick, C. L. Water-Soluble Polymers. 81. Direct Synthesis of Hydrophilic Styrenic-Based Homopolymers and Block Copolymers in Aqueous Solution via RAFT. *Macromolecules* **2001**, *34*, 2248−2256.
(48) Zhang, Y.; Wang, Z.; Matyjaszewski, K.; Pietrasik, J. Evolution of Morphology of POEGMA-*b*-PBzMA Nano-Objects Formed by PISA. *Macromol. Rapid Commun.* **2019**, *40*, No. 1800331.
(49) Dudek, T. J.; Lohr, J. J. Glass transition temperatures of poly(methyl methacrylate) plasticized with low concentrations of monomer and diethyl phthalate. *J. Appl. Polym. Sci.* **1965**, *9*, 3795−3818.
(50) György, C.; Verity, C.; Neal, T. J.; Rymaruk, M. J.; Cornel, E. J.; Smith, T.; Growney, D. J.; Armes, S. P. RAFT Dispersion Polymerization of Methyl Methacrylate in Mineral Oil: High Glass Transition Temperature of the Core-Forming Block Constrains the Evolution of Copolymer Morphology. *Macromolecules* **2021**, *54*, 9496−9509.
(51) Chan, D. H. H.; Cockram, A. A.; Gibson, R. R.; Kynaston, E. L.; Lindsay, C.; Taylor, P.; Armes, S. P. RAFT Aqueous Emulsion Polymerization of Methyl Methacrylate: Observation of Unexpected Constraints When Employing a Non-Ionic Steric Stabilizer Block. *Polym. Chem.* **2021**, *12*, 5760−5769.
(52) Fuchise, K.; Sone, M.; Miura, Y.; Sakai, R.; Narumi, A.; Sato, S.; Satoh, S.; Kakuchi, T. Precise synthesis of poly(1-adamantyl methacrylate) by atom transfer radical polymerization. *Polym. J.* **2010**, *42*, 626−631.
(53) Goh, S. H. Miscible blends of poly(tetrahydrofurfuryl methacrylate) with two hydroxyl-containing polymers. *Polym. Bull.* **1987**, *17*, 221−224.
(54) Sugihara, S.; Hashimoto, K.; Okabe, S.; Shibayama, M.; Kanaoka, S.; Aoshima, S. Stimuli-Responsive Diblock Copolymers by Living Cationic Polymerization: Precision Synthesis and Highly Sensitive Physical Gelation. *Macromolecules* **2004**, *37*, 336−343.


https://doi.org/10.1021/acsomega.2c03440
*ACS Omega* 2022, 7, 26894−26904